

MGCN: Descriptor Learning using Multiscale GCNs

YIQUN WANG, NLPR, CASIA & School of AI, Univ. of CAS

JING REN, KAUST

DONG-MING YAN, NLPR, CASIA & School of AI, Univ. of CAS

JIANWEI GUO, NLPR, CASIA & School of AI, Univ. of CAS

XIAOPENG ZHANG, NLPR, CASIA & School of AI, Univ. of CAS

PETER WONKA, KAUST

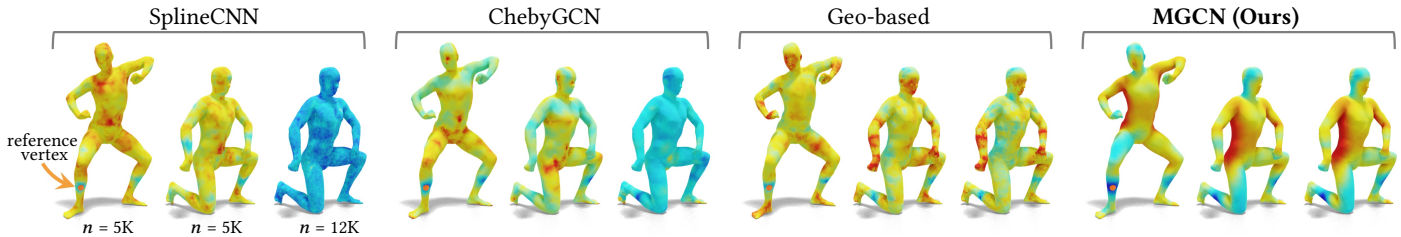


Fig. 1. Visualization of dissimilarity maps. For a vertex highlighted by the orange arrow, we take its learned descriptor and visualize the difference to other vertex descriptors on the same shape, another shape with the same 5K resolution, and the other shape in a different 12.5K resolution. We compare four different learned descriptors, from left to right: SplineCNN, ChebyGCN, Geodesic-based method [2019a], and MGCN. All networks are trained on 5K and tested on 5K and 12.5K resolution. We can see that our network MGCN is most consistent between different resolutions.

We propose a novel framework for computing descriptors for characterizing points on three-dimensional surfaces. First, we present a new non-learned feature that uses graph wavelets to decompose the Dirichlet energy on a surface. We call this new feature *wavelet energy decomposition signature* (WEDS). Second, we propose a new *multiscale graph convolutional network* (MGCN) to transform a non-learned feature to a more discriminative descriptor. Our results show that the new descriptor WEDS is more discriminative than the current state-of-the-art non-learned descriptors and that the combination of WEDS and MGCN is better than the state-of-the-art learned descriptors. An important design criterion for our descriptor is the robustness to different surface discretizations including triangulations with varying numbers of vertices. Our results demonstrate that previous graph convolutional networks significantly overfit to a particular resolution or even a particular triangulation, but MGCN generalizes well to different surface discretizations. In addition, MGCN is compatible with previous descriptors and it can also be used to improve the performance of other descriptors, such as the heat kernel signature, the wave kernel signature, or the local point signature.

CCS Concepts: • **Computing methodologies** → **Shape analysis**.

Additional Key Words and Phrases: Multiscale, Energy Decomposition, Wavelet Convolution

1 INTRODUCTION

Designing descriptors for surface points is a fundamental problem in geometry processing as descriptors are a building block for many applications, such as shape matching, registration, segmentation, and retrieval.

A good descriptor should satisfy two criteria: (1) the descriptor should be *discriminative* to map similar surface points to similar

values and dissimilar surface points to dissimilar values. The definition of similarity depends on the application. In our setting, we consider the very popular requirement that descriptors should be invariant to rigid and near-isometric deformations of the surface. (2) the descriptor should be *robust* to different discretizations of the surface, e.g., meshes of different resolution and triangulation. If the descriptor discriminates surface points based on the discretization, we also say it overfits or lacks generalization.

Generally, we can distinguish two types of descriptor computation: supervised and unsupervised. Examples of unsupervised descriptors are the *wave kernel signature* (WKS) and the *heat kernel signature* (HKS). While these descriptors are robust to different surface discretization, there is a lot of room for improvement making them more discriminative. This can be done successfully using neural networks to compute supervised descriptors. A very promising type of network architecture are graph convolutional networks, such as chebyGCN [Defferrard et al. 2016], GCN [Kipf and Welling 2017], SplineCNN [Fey et al. 2018], and DGCNN [Wang et al. 2019b]. Even though many of these networks have not been applied to descriptor learning directly, their adaption to descriptor learning only requires little effort. However, the current state of the art is typically not robust to different surface discretizations and overfits. See Fig. 1 for an illustration. One main reason for this overfitting is that the convolution operation typically depends on a k -ring neighborhood of a surface point. This changes the spatial support of a convolutional filter if, for example, the resolution of the underlying surface triangulation changes. One possible approach to make descriptor learning robust to different resolutions is to resample the surface. This approach has other drawbacks, such as the additional complexity of resampling and the loss of information reducing the discrimination performance.

Authors' addresses: Yiqun Wang, NLPR, CASIA & School of AI, Univ. of CAS, yiqun.wang@nlpr.ia.ac.cn; Jing Ren, KAUST, jing.ren@kaust.edu.sa; Dong-Ming Yan, NLPR, CASIA & School of AI, Univ. of CAS, yandongming@gmail.com; Jianwei Guo, NLPR, CASIA & School of AI, Univ. of CAS, jianwei.guo@nlpr.ia.ac.cn; Xiaopeng Zhang, NLPR, CASIA & School of AI, Univ. of CAS, xiaopeng.zhang@ia.ac.cn; Peter Wonka, KAUST, pwonka@gmail.com.

In this paper, we propose contributions to unsupervised and supervised descriptor computation leveraging the power of wavelets. For the learning part, we introduce a novel graph convolutional network called *Multiscale Graph Convolutional Network* (MGCN). Our results will show significant improvements to descriptor performance even when tested under a variety of different surface discretizations. The key novelty of our network is a convolution operation expressed in the wavelet basis. This lets us define a multiscale convolution with filters of both local and global support.

For the unsupervised descriptor computation part, we theoretically derive a novel local spectral feature called *Wavelet Energy Decomposition Signature* (WEDS) from the Dirichlet energy. Different from traditional spectral descriptors (e.g., *Global Point Signature* (GPS), *Heat Kernel Signature*, and *Wave Kernel Signature*), we introduce additional vertex coordinate information to capture more distinctive attributes. Compared with *Local point signature* (LPS) [Wang et al. 2019a], our new descriptor uses wavelets to capture both local and global information, which is more discriminative.

Our extensive experimental evaluations indicate that the WEDS descriptor outperforms recent state-of-the-art unsupervised descriptors. Further, WEDS can be combined with MGCN to improve upon the currently best supervised descriptors. Besides the traditional evaluation of descriptor performance with respect to rigid, isometric, and near-isometric surface deformations we also evaluate the robustness to different surface discretizations.

The main contributions of this work are as follows:

- We design a new graph convolutional network named *Multiscale Graph Convolutional Network* (MGCN). While we focus on descriptor learning as main application, the robustness to resolution of our new convolution layer holds promise for many additional applications.
- We present a novel multiscale feature called *Wavelet Energy Decomposition Signature* (WEDS) based on energy decomposition that improves upon state-of-the-art unsupervised descriptors.

2 RELATED WORK

We review related work for descriptor computation in three categories and subsequently related work for graph convolutional neural networks.

Spatial domain approaches. Descriptors directly constructed in the spatial domain often rely on histograms. *Spin images* (SI) [Johnson and Hebert 1999] and *3D shape context* (3DSC) [Frome et al. 2004] are generated by creating accumulators, which divide the local space into different bins and calculate the number of points that fall into each bin. *Signature of histogram of orientations* (SHOT) [Tombari et al. 2010] is constructed by accumulating the normal angles of the key and neighboring points in the neighborhood space. Unlike the SHOT descriptor, the MeshHOG [Zaharescu et al. 2009] descriptor is another histogram based on the orientations of the gradients on the mesh. The *rotational projection statistics* (RoPS) [Guo et al. 2013] descriptor is generated by rotationally projecting neighboring points onto 2D planes and calculating a set of statistics. Spatial domain descriptors generally have the following performance characteristics. First, they heavily rely on local information, but do not

capture global information. Second, the descriptors are sensitive to the discretization of the surface. While this is desirable for some applications, an important goal of our work is to be robust to different surface discretizations.

Spectral domain approaches. Many spectral descriptors have been proposed to deal with isometric deformations. Especially popular are intrinsic descriptors based on the Laplace–Beltrami operator. Shape–DNA [Reuter et al. 2006] considers the spectrum of the Laplace–Beltrami operator as the descriptor because the spectrum is isometry-invariant and independent of spatial position. GPS [Rustamov 2007] combines the spectrum and eigenfunctions to obtain a descriptor on each vertex. HKS [Sun et al. 2010], scale-invariant HKS [Bronstein and Kokkinos 2010], and WKS [Aubry et al. 2011] were proposed based on diffusion geometry. The intrinsic properties make the descriptors invariant to isometric deformation. LPS [Wang et al. 2019a] combine coordinate information and intrinsic geometric information to get a more robust descriptor. The discrete time evolution process (DTEP) descriptor [Melzi et al. 2018] focuses on non-isometric deformations and achieved better results. But these methods take a lot of time to compute geodesic distances or solve optimization problems. In our results, we compare to the best performing descriptors to demonstrate an important improvement in performance. Our discussion in Section 4.5 will explain why we are able to beat the state of the art in more detail.

Deep learning approaches. We call the descriptors reviewed in the previous two sections to be unsupervised. By contrast, supervised descriptors use supervised learning, mainly deep learning, to extract shape descriptors. Wei et al. [2016] generate descriptors by using a large dataset of depth maps for training. Huang et al. [2018] extract local descriptors by training on multiple rendered views in multiple scales. Zeng et al. [2017] use 3D volumetric convolutional neural networks to generate local descriptors for robustly matching RGB-D data. The method of *compact geometric features* (CGF) [Khoury et al. 2017] maps high-dimensional histograms into a low-dimensional Euclidean space to generate descriptors on unstructured point clouds. Deng et al. [2018] found matches in unorganized point clouds by adapting the PointNet architecture. Although these methods have obtained good results through learning, they do not make full use of the structure of 3D data. Multi-view based methods must solve the problem of occlusion. Voxel-based methods consume a lot of resources and cannot explore the details of an object. Learning methods that work by feeding point cloud coordinates or histogram features into multi-layer perceptrons are currently not able to extract enough important information from the data.

Some other descriptors are generated by exploiting the correlation between local points in the frequency domain or spatial domain. *Optimal spectral descriptors* (OSD) [Litman and Bronstein 2014] are constructed by learning parametric filters in the spectral domain. Boscaini et al. [2015] generalize the windowed Fourier transform to learn local shape descriptors on manifolds. *Anisotropic diffusion descriptors* [Boscaini et al. 2016] based on anisotropic diffusion are constructed by using a fully connected neural network to learn the kernel filters. In the spatial domain, Masci et al. [2015] design a geodesic convolutional network to learn shape descriptors on manifolds by extracting and regularly charting geodesic local patches and designing a patch operator for convolution. Wang et

al. [2018] employ a deep learning framework by projecting geodesic local patches into local geometry images to learn descriptors. Subsequently, LPS [Wang et al. 2019a] is proposed on geodesic local patches and used with deep learning to construct a more discriminative descriptor. Although these spatial domain methods can convolve local regions on manifolds and get better results, they need to extract local geodesic patches, which is very time-consuming. In addition, it is very difficult to maintain a disk topology if the local region becomes larger and the surface contains topological holes.

Graph convolutional network. Recently, a large number of graph convolutional learning methods have emerged. This learning method has achieved high performance on irregular data. Spectral CNN [Bruna et al. 2014] is the first to perform convolution operations on the graph through a frequency domain transform. ChebyGCN [Deferrard et al. 2016] simplifies spectral CNN by designing spectral filters using a k -order polynomial parametrization. GCN [Kipf and Welling 2017] further simplifies polynomials to 1-order and is suitable for semi-supervised learning. SplineCNN [Fey et al. 2018] uses B-Spline Kernels to weight the relationship between a point and its neighborhood. Although this network has strong fitting ability, the generalization is not strong as the pseudo-coordinates on the edges are not invariant to rigid transformations. Wang *et al.* [2019b] present a *dynamic graph* CNN (DGCNN) on point cloud, which can build dynamic connections by selecting a k -neighborhood in feature space. The problem with the graph convolution using a 1-neighborhood or k -neighborhood is that it is not applicable to the case of multi-resolution because the size of the receptive field is different when applying different discretizations. The graph wavelet neural network [Xu et al. 2019] uses the wavelet transform to formulate convolutions on a graph. The problem with this convolution method is that only a single-scale wavelet is used in the transformation. In addition, the number of filters in this algorithm is related to the number of vertices, so that convolution in multiple resolutions cannot be achieved.

Even though there are many methods of graph convolutional networks, a graph convolutional network is rarely used to learn shape descriptors. One of the problems is that graph convolutions are strongly influenced by the neighborhood relationships stemming from the surface discretization. Therefore, the result is overly sensitive to the discretization of the surface. We focus on the issues of resolution and triangulation in graph convolutional networks and present a novel network to generate an informative descriptor that is robust to the change of resolution and triangulation.

3 PROBLEM STATEMENT AND OVERVIEW

Given is a mesh \mathcal{M} as discretization of an underlying smooth two-manifold surface defined as (V, E) , where $V = \{v_i | i = 1, \dots, N\}$ and E are the sets of vertices and edges, respectively. The vertex coordinates are defined by the function $X = (x_1, x_2, x_3) : V \rightarrow \mathbb{R}^3$. Our goal is to compute a local descriptor $f(v_i) \in \mathbb{R}^d$ for any given vertex v_i .

The local descriptor is generated in two stages: unsupervised descriptor computation and supervised descriptor learning. At the first stage, we compute our proposed descriptor WEDS for each vertex

in the wavelet domain that is robust to the change of resolution, triangulation, scale, and rotation. The second stage is about descriptor learning. Inspired by the derivation of WEDS, we propose a graph convolutional network called MGCN to generate better descriptors from WEDS. Benefiting from the expressiveness of graph wavelets, our network can be trained on one resolution and tested on other resolutions without significant reduction of performance.

4 UNSUPERVISED DESCRIPTOR COMPUTATION

In this section, we first review Laplacian eigenfunctions and graph wavelets. Then, we propose a new type of shape descriptor, WEDS. Finally, we discuss properties and advantages of WEDS.

4.1 Laplacian Eigenfunctions

Let \mathcal{S} denote a continuous surface. We can find an orthonormal basis on \mathcal{S} , containing the k smoothest possible functions that are orthogonal to each other, by finding the first k eigenfunctions of Δ [Bronstein et al. 2017], the Laplace–Beltrami operator:

$$\Delta \phi_i = \lambda_i \phi_i, i = 0, 1, \dots, k - 1, \quad (1)$$

where $\{\lambda_i | i = 0, 1, \dots, k - 1\}$ are the smallest k eigenvalues in increasing order. To simplify the notation, we use the same variable names for discrete and continuous settings. The difference should be clear from the context.

In the discrete setting of a triangulated mesh \mathcal{M} with n vertices, we can discretize the Laplace–Beltrami operator as follows:

$$\mathbf{L}\phi_i = \lambda_i \mathbf{A}\phi_i, i = 0, 1, \dots, k - 1, \quad (2)$$

where \mathbf{L} is a standard cotangent Laplacian matrix with size $n \times n$, \mathbf{A} is the $n \times n$ diagonal area matrix. ϕ_i is a $n \times 1$ vector, the eigenvector w.r.t. the eigenvalue λ_i . Also, note that for the generalized eigenvalue problem, the eigenvectors ϕ_i are orthogonal to each other in terms of the \mathbf{A} -dot product.

$$\left\langle \phi_i, \phi_j \right\rangle_{\mathbf{A}} = \phi_i^T \mathbf{A} \phi_j. \quad (3)$$

Any function f defined on a smooth surface can be expressed as a weighted combination of the eigenfunctions:

$$f = \sum_{j=0}^{+\infty} \sigma_j \phi_j, \quad (4)$$

where σ_j is the coefficient corresponding to the j^{th} eigenfunction. In the discrete case, the coefficients can be calculated by

$$\sigma_j = \left\langle \mathbf{f}, \phi_j \right\rangle_{\mathbf{A}} = \mathbf{f}^T \mathbf{A} \phi_j, \quad (5)$$

where \mathbf{f} is the corresponding discretization of a smooth function f that is defined on the vertices of a triangulated mesh.

We can see that with the help of basis functions, a function on the surface can be transformed into a set of coefficients. Graph wavelets, explained next, make use of the same idea. The main difference is that instead of eigenfunctions of the Laplace–Beltrami operator, wavelet and scaling functions are used as basis functions.

4.2 Graph Wavelets

We build on the graph wavelet framework described in paper by Hammond et al. [2011]. To make the application specific to meshes using the cotangent Laplacian rather than the uniform Laplacian we build on the notation of [Masoumi and Hamza 2017] where the inner product is defined with respect to the area matrix \mathbf{A} .

Wavelet function. One graph wavelet function $\psi_{t,\mathbf{v}}$ is defined per vertex v per time scale t . We denote the number of time scales as K (K is typically less than 100). To construct a wavelet function, a filter function g is used. Examples for g are the Mexican hat or cubic splines. Let $a(v)$ be the Voronoi area at vertex v and $\phi_j(v)$ be the element of vector ϕ_j corresponding to vertex v . Then $\psi_{t,\mathbf{v}}$, the spectral graph wavelet localized at vertex v and scale t , is given by

$$\psi_{t,\mathbf{v}} = \sum_{j=0}^{N-1} a(v) g(t\lambda_j) \phi_j(v) \phi_j. \quad (6)$$

We show examples in Fig. 2 to demonstrate the local property of wavelets.

To project a given function \mathbf{f} onto the wavelet basis, we compute the inner product between the wavelet functions and the given function \mathbf{f} . The spectral graph wavelet coefficients are then defined as:

$$W_{\mathbf{f}}(t, v) = \langle \mathbf{f}, \psi_{t,\mathbf{v}} \rangle_{\mathbf{A}} = \sum_{j=0}^{N-1} a(v) g(t\lambda_j) \sigma_j \phi_j(v). \quad (7)$$

Scaling function. In addition to the graph wavelet functions, there is a single scaling function $\xi_{\mathbf{v}}$ defined per vertex v on the surface. The scaling function is defined via a filter function $h(x)$. Typically, $h(x)$ is the same type of function as $g(x)$, but using different parameters. The scaling function captures low-frequency information and is given by

$$\xi_{\mathbf{v}} = \sum_{j=0}^{N-1} a(v) h(\lambda_j) \phi_j(v) \phi_j. \quad (8)$$

An illustration is shown in Fig. 2. Similar to the wavelet functions, we compute the inner product between a given function \mathbf{f} and the scaling functions to obtain the scaling function coefficients

$$S_{\mathbf{f}}(v) = \langle \mathbf{f}, \xi_{\mathbf{v}} \rangle_{\mathbf{A}} = \sum_{j=0}^{N-1} a(v) h(\lambda_j) \sigma_j \phi_j(v). \quad (9)$$

To use graph wavelets in our framework, the filter functions $g(x)$ and $h(x)$ cannot be chosen arbitrarily, as we require that they form a Parseval frame [Stanković and Sejdić 2019]. This is necessary so that the coefficients can be used to recover the original signal in the discrete case as follows:

$$\mathbf{f} = \sum_{m=1}^K \sum_{\mathbf{v}} a(v)^{-1} W_{\mathbf{f}}(t_m, v) \psi_{t_m, \mathbf{v}} + \sum_{\mathbf{v}} a(v)^{-1} S_{\mathbf{f}}(v) \xi_{\mathbf{v}}, \quad (10)$$

where t_m is the m^{th} scale of the wavelet function. We will discuss Parseval frames and the choice of filter functions in Section 4.4.

The formula can be simplified as

$$\mathbf{f} = \sum_{m=0}^K \sum_{\mathbf{v}} a(v)^{-1} W_{\mathbf{f}}(t_m, v) \psi_{t_m, \mathbf{v}}, \quad (11)$$

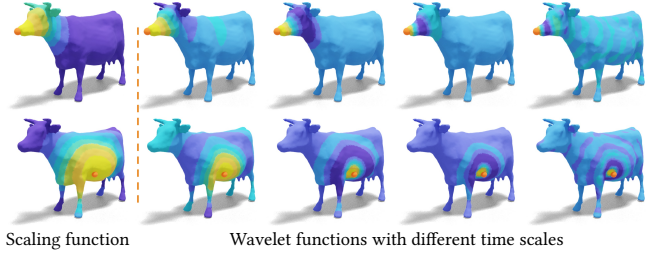


Fig. 2. Illustration of wavelet functions and scaling functions. The top row corresponds to a vertex on the mouth and the bottom row to a vertex on the stomach (shown as orange spheres). The first column shows the scaling functions $\xi_{\mathbf{v}}$ corresponding to the vertices. The second to fifth columns correspond to wavelet functions $\psi_{t,\mathbf{v}}$ of different time scales $t = 0.0210$, $t = 0.0102$, $t = 0.0024$, and $t = 5.59e-4$.

where $W_{\mathbf{f}}(t_0, v) = S_{\mathbf{f}}(v)$, and $\psi_{t_0, \mathbf{v}} = \xi_{\mathbf{v}}$. The proof is given in the appendix.

4.3 Wavelet Energy Decomposition Signature

To derive our new descriptor, we combine multiple ideas. First, we would like to start from the coordinate functions $\mathbf{X} = (\mathbf{x}_1, \mathbf{x}_2, \mathbf{x}_3)$, because they completely describe the shape and are therefore very informative. Second, to make this information invariant to rigid transformations, we employ the sum of the Dirichlet energy of the three coordinate functions. This summation equals to the surface area and the computation of the Dirichlet energy is generally robust to different discretizations. Third, to aggregate local information in an area around the vertex, we employ graph wavelets at different scales described previously. This ensures that our descriptor is more discriminative than current state-of-the-art descriptors.

Given a smooth real-valued function $f : \mathcal{S} \rightarrow \mathbb{R}$ defined on the surface, the Dirichlet energy measures how smooth the function f is over the surface \mathcal{S} :

$$E(f) = \int_{\mathcal{S}} |\nabla f(v)|^2 dv = \int_{\mathcal{S}} f(v) \Delta f(v) dv. \quad (12)$$

In its discrete form, the Dirichlet energy is computed as $\mathbf{f}^T \mathbf{ALF}$. Combined with Equations (1) (7) (6) and (11), the Dirichlet energy of the function can be expressed in the graph wavelet basis as follows:

$$E(\mathbf{f}) = \mathbf{f}^T \mathbf{ALF} = \sum_{j=0}^{N-1} \lambda_j \left(\sum_{m=0}^K \sum_{\mathbf{v}} \gamma_j(t_m, v) \right)^2, \quad (14)$$

where $\gamma_j(t_m, v) = W_{\mathbf{f}}(t_m, v) g_{t_m}(\lambda_j) \phi_j(v)$ and N is the number of vertices. We define $g_{t_m}(\lambda_j)$ as follows:

$$g_{t_m}(\lambda_j) = \begin{cases} h(\lambda_j), & \text{if } m = 0 \\ g(t_m \lambda_j), & \text{if } m > 0 \end{cases} \quad (15)$$

The Dirichlet energy of a vector-valued function $\mathbf{F} = (\mathbf{f}_1, \mathbf{f}_2, \dots, \mathbf{f}_d) : V \rightarrow \mathbb{R}^d$ on the mesh is defined as the sum of the Dirichlet energy of the individual components:

$$E(\mathbf{F}) = \sum_{i=1}^d E(\mathbf{f}_i). \quad (16)$$

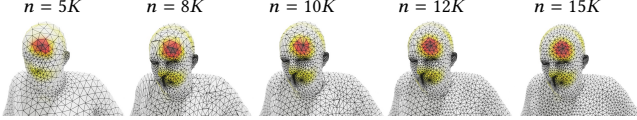


Fig. 3. We choose five resolutions to show the wavelet function on one vertex. From left to right: 5K, 8K with random filpping, 10K, 12K, 15K. The model with 5K vertices is remeshed and 8K is with random filpping. From the illustration, the wavelet functions are robust w.r.t. change of resolution and triangulation.

Now, we substitute the coordinate functions $\mathbf{X} = (\mathbf{x}_1, \mathbf{x}_2, \mathbf{x}_3) : V \rightarrow \mathbb{R}^3$ into the Equation (16) above and express the result in the wavelet basis following Equation (14):

$$E(\mathbf{X}) = \sum_{i=1}^d \sum_{j=0}^{N-1} \lambda_j \sum_{m=0}^K \sum_v \gamma_{ij}(t_m, v) \omega_{ij} \quad (17)$$

$$= \sum_{m=0}^K \sum_v \sum_{j=0}^{N-1} \lambda_j \sum_{i=1}^d \gamma_{ij}(t_m, v) \omega_{ij}, \quad (18)$$

where $\omega_{ij} = \sum_{m=0}^K \sum_v \gamma_{ij}(t_m, v)$.

The Dirichlet energy of this generalized function can be decomposed into different scale energies $\sum_{j=0}^{N-1} \lambda_j \sum_{i=1}^d \gamma_{ij}(t_m, v) \omega_{ij}$ on each vertex.

In addition, we ignore the first term when $j = 0$ since the first eigenvalue of a mesh $\lambda_0 = 0$. The Dirichlet energy can be decomposed into K multiscale vectors with lengths equal to the number of vertices and can be expressed as:

$$\boldsymbol{\varepsilon}_{t_m} = \left\{ \sum_{j=1}^{N-1} \lambda_j \sum_{i=1}^d \gamma_{ij}(t_m, v) \omega_{ij} \right\}, m \in [0, K]. \quad (19)$$

After energy decomposition, the amount of energy of an individual vertex depends on the number of vertices on the surface. Because the Dirichlet energy of a shape with different resolutions or discretizations is constant, the higher the resolution of a mesh is, the less energy each vertex has. To get features of similar scale at a surface point when the underlying discretization changes, we need to collect local energy at each vertex to form our signature. Finding the geodesic neighbors of a surface point is very time-consuming. Fig. 3 shows the wavelet basis functions at the meshes of different resolutions. We find that the shape of the wavelet does not change significantly on the meshes of different resolutions, which can be used to weight different resolutions of meshes. Thanks to the natural local properties of graph wavelets, the local wavelets can be used to collect the local energy to compute our signature on different resolutions. A wavelet $\psi_{t_s, v}$ at a particular vertex can be thought of as the associated weights of points with the particular vertex. The weights of points are significant when the points near the specific vertex when measured by geodesic distance, and the influence is small if points is far from the vertex. For one scale t_s and every vertex v , we first normalize the wavelet $\psi_{t_s, v}$ to obtain a normalized vector $\boldsymbol{\psi}_{t_s, v^*}$ using *max - min* normalization. Then, we use

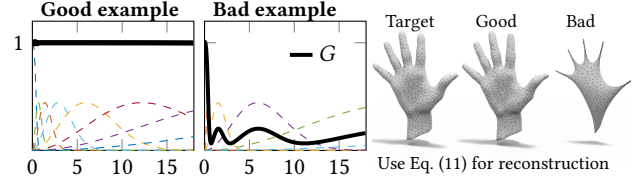


Fig. 4. We show two choices of filters (dashed lines) and the function G defined in Eq. (22) (solid black line). We then use these two sets of filters to reconstruct a hand shape, i.e., use Eq. (11) to reconstruct the 3D coordinate functions. We can see that for the bad filter choice, where the constraint $G = 1$ is not satisfied, the reconstruction quality is very poor. On the other hand, the good filters can better reconstruct the given signal.

normalized vector $\boldsymbol{\psi}_{t_s, v^*}$ to weight energy $\boldsymbol{\varepsilon}_{t_m}$. The formula of our signature on one vertex v at one scale t_s is expressed as follows:

$$WEDS_{t_s}(v) = \left\{ \sum_x \boldsymbol{\psi}_{t_s, v}^*(x) \boldsymbol{\varepsilon}_{t_m}(x) \right\}, m \in [0, K]. \quad (20)$$

To obtain scale invariance, the energy vectors $\boldsymbol{\varepsilon}_t$ are modified by multiplying its eigenvalue λ_j like LPS [Wang et al. 2019a]. Therefore, $\boldsymbol{\varepsilon}_{t_m} = \left\{ \sum_{j=1}^{N-1} \lambda_j^2 \sum_{i=1}^d \gamma_{ij}(t_m, v) \omega_{ij} \right\}$. To construct our vertex descriptor, the weighting approach with one wavelet scale is not discriminative. Therefore, we cascaded the descriptors at different scales in the scale set S_{t_s} . We will mention how to select scales in Section 4.4.

$$WEDS(v) = \{WEDS_{t_s}(v)\}, t_s \in S_{t_s} \quad (21)$$

4.4 Multiscale Filters

If an original signal can be recovered by a graph wavelet basis (recall Equation (10)), the filters need to satisfy the Parseval frame,

$$G(\lambda_j) = h^2(\lambda_j) + \sum_{m=1}^K g^2(t_m \lambda_j) \equiv 1, \quad (22)$$

and the proof is given in appendix. Fig. 4 visualizes the importance of constraint G . We show two choices of filter functions, one that does and one that does not satisfy this constraint. We choose Mexican hat functions as the filters of the graph wavelet, and they are given by:

$$g(t_m \lambda_j) = A(t_m \lambda_j)^2 e^{(1 - (t_m \lambda_j)^2)} \quad (23)$$

$$h(\lambda_j) = B e^{-\left(\frac{C \lambda_j}{\lambda_{\max}}\right)^3}, \quad (24)$$

where $t_m = e^{\text{linspace}(\log(\frac{D}{\lambda_{\max}}), \log(\frac{E}{\lambda_{\max}}), K)}$. Considering the balance of efficiency and accuracy, in our tests, we choose 32 wavelet filters, i.e., $K = 31$. We set the tolerance to 0.01, and the five parameters can be solved: $A = 0.443, B = 1.004, C = 38.462, D = 46, E = 0.2$.

For the scale set S_{t_s} , the selection is based on the number of dimensions generated by the features on each vertex. For one scale in S_{t_s} , we can generate 32-dimensional features. So WEDS can generate



Fig. 5. We show WEDS on two different shapes with different pose and resolution. We show 8 different dimensions of our descriptors. We can see that WEDS is robust w.r.t. the triangulation and resolution.

Table 1. The discrete Dirichlet energy $E(\mathbf{f})$ of the vertex coordinate functions or the WKS functions.

$E(\mathbf{f})$	Res	Dims1	Dims2	Dims3	SUM	Area*2
of Coord	6890	1.0153	1.4768	1.1114	3.6035	3.6035
	10K	1.0156	1.4716	1.1092	3.5964	3.5964
	15K	1.0135	1.4719	1.1061	3.5915	3.5915
$E(\mathbf{f})$	Res	Dims1	Dims2	Dims3	Dims4	SUM
	6890	0.7645	2.9629	4.8548	4.0352	12.6174
	10K	0.7639	2.9764	4.8979	4.0372	12.6754
15K	0.7581	2.9836	4.7605	4.0883	12.5905	

features with a maximum of 1024 dimensions. But high-dimensional features are usually not needed. To represent high, medium, and low frequencies, we select at least 3 scales, and features with at least 96 dimensions are generated, after which we can obtain fewer dimensions by sampling. If more dimensions of feature need to be generated, then more scales need to be picked. We take a linear sampling approach and remove the first and last filters, which is as follows:

$$S_{t_s} = \left\{ t_m, m = \left\lfloor \text{linspace}(32, 1, \left\lfloor \frac{\text{Num}}{32} \right\rfloor + 2) \right\rfloor (2 : \text{end} - 1) \right\}. \quad (25)$$

where Num is the feature dimension of the output. In Fig. 5, we show our WEDS descriptors on two shapes with 8 selected dimensions.

4.5 Discussion

Many spatial and spectral descriptors have been proposed, but these descriptors only satisfy the expected property simultaneously, such as resolution, scale, and discrimination. Our goal is to find a new descriptor that can be discriminative and robust to different shape structure at the same time. We are inspired by the following observation: for a smooth surface \mathcal{S} to any triangulated mesh \mathcal{M} with any resolution. If a discrete vector \mathbf{f} is sampled from a smooth function f , the discrete Dirichlet energy $E(\mathbf{f}) = \mathbf{f}^T \mathbf{A} \mathbf{f}$ is robust to discretization. Table 1 shows two smooth function, which is vertex coordinate and WKS. It can be found that the discrete Dirichlet energy on every dimension and its sum on this two smooth functions are robust to the change of resolution. In addition, Dirichlet energy is invariant to a rigid transformation, which is very important in feature design. Therefore, we want to derive a set of descriptors from the Dirichlet energy of a given function \mathbf{f} . An interesting phenomenon is that the Dirichlet energy of vertex coordinates has been proved to be twice

of surface area of the mesh, and the surface area is very robust to different discretization. The coordinates are also the most primitive and comprehensive information of given shape, so we choose the vertex coordinate function as input. To have other desirable properties, we just need to pick a different function \mathbf{f} .

To derive a set of per-vertex descriptors from this energy, we need to distribute the energy of the function \mathbf{f} to the vertices. One trivial solution is simply use the Laplacian–Beltrami basis, where we can project function \mathbf{f} to the Laplacian–Beltrami basis like Equation (5). However, in this case, we only have σ_j that characterize the global attributes of the shape. One possible way to get local features for each vertex is to cut a geodesic disk like LPS [Wang et al. 2019a] and compute the Dirichlet energy locally, but it is time-consuming and does not contain global information.

Another choice is to distribute the energy of \mathbf{f} using the graph wavelet basis, which are a set of basis defined on each of the vertices. In this case, the wavelet basis can capture the local details in a spatial region around the vertex. In addition, wavelets on graphs are expressed using eigenfunctions of the Laplacian–Beltrami operator, and we can project function \mathbf{f} to the wavelet basis and get the coefficients in Equation (7). After projection, it can be found that the wavelet coefficient $W_{\mathbf{f}}(t, v)$ contains the coefficient σ_j which include global information of \mathbf{f} . Because the coefficients of graph wavelets can capture both global and local information, the reconstructed energy of \mathbf{f} can be distributed to each vertex while maintaining the global and local information at the same time. Therefore, we derive a descriptor with high discrimination while maintaining robustness. To sum up, wavelets enable us to achieve a trade-off between local and global information that other descriptors are unable to achieve.

5 SUPERVISED DESCRIPTOR LEARNING

We propose a new graph convolutional network called MGCN. We mainly employ MGCN for descriptor learning in this paper, but it is a general architecture for graph convolutional networks. We first describe a single layer of our network in Section 5.1, and then the complete architecture and training details in Section 5.2.

5.1 Multiscale Graph Convolution Layer

A layer of our network takes a C -dimensional vector for each of the N graph nodes as input and outputs an O -dimensional vector for each node. For simplicity of notation, we start the description by considering the case of $C = O = 1$ and extend to higher dimensions in the end. We also focus on discrete descriptions for simplicity. Under this simplifying assumption, we denote the input as signal $\mathbf{x}^{\text{in}} \in \mathbb{R}^N$ and the output as $\mathbf{x}^{\text{out}} \in \mathbb{R}^N$. The goal of our layer is to convolve the signal \mathbf{x} with a filter $\mathbf{y} \in \mathbb{R}^N$, i.e., to compute $\mathbf{y} *_w \mathbf{x}$ where $*_w$ is the convolution operator. Convolution in the time domain is equal to the product in the frequency domain. Following previous work, we consider spectral convolutions on graphs defined as

$$\mathbf{x}^{\text{out}} = \mathbf{y} *_w \mathbf{x}^{\text{in}} = \Phi \left(\left(\Phi^T \mathbf{y} \right) \odot \left(\Phi^T \mathbf{x}^{\text{in}} \right) \right) = \Phi \mathbf{w}_\theta \Phi^T \mathbf{x}^{\text{in}}, \quad (26)$$

where \odot is the element-wise product, $\Phi \in \mathbb{R}^{N \times k}$ is an eigenvector matrix, and $\mathbf{w}_\theta \in \mathbb{R}^{k \times k}$ is a diagonal matrix describing the filter

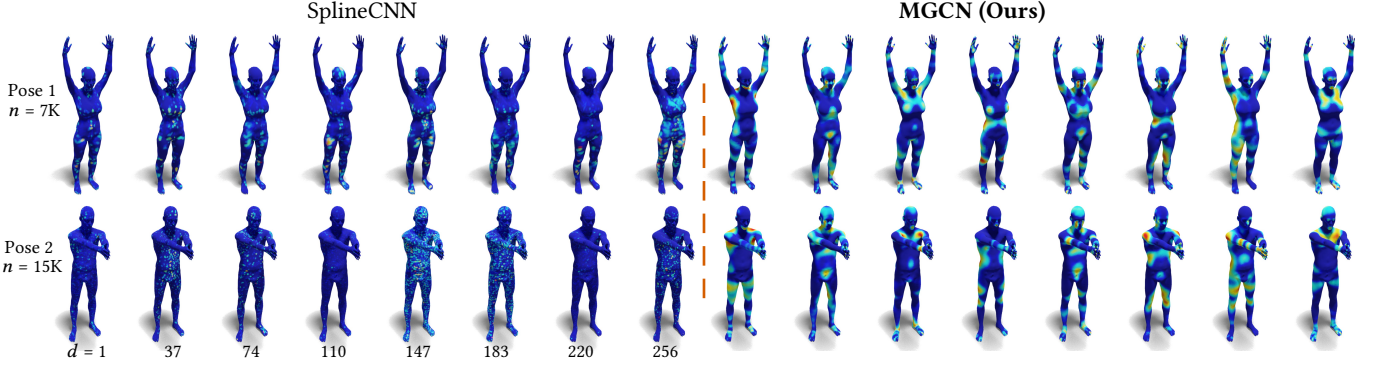


Fig. 6. We train SplineCNN and our MGCN on the WEDS descriptors as visualized in Fig. 5 and show the learned descriptors on the same shape and same dimension. We can see that, though the learned descriptors from SplineCNN has reasonable accuracy in shape matching, the learned descriptors are not smooth and do not encode any semantic information. As a comparison, the learned descriptors from our network are much more coherent between shapes with different pose and resolution. Also our learned descriptors are more smooth.

in the frequency domain. In general, \mathbf{w}_θ can be considered to be a function of the eigenvalue matrix Λ , i.e., $\mathbf{w}_\theta = f(\Lambda)$. To improve efficiency, ChebyNet [Defferrard et al. 2016] approximates the arbitrary function f as weighted sum of powers of Λ :

$$\mathbf{w}_\theta = \sum_{m=0}^{K-1} \theta_m \text{diag}(\{\lambda_j\}_{j=0}^{k-1})^m = \sum_{m=0}^{K-1} \theta_m \Lambda^m, \quad (27)$$

where Λ is a diagonal matrix of size $K \times K$, and the elements on the diagonal are eigenvalues λ_j .

In this way, the convolution can be replaced by a linear combination of m -order polynomials of the Laplacian matrix, which eliminates the need to calculate the eigenfunctions. Laplacians with order m are m -localized. For efficient computation, Chebyshev polynomials are computed recursively as follows:

$$\mathbf{x}^{\text{out}} = \mathbf{y} * \mathbf{w} \mathbf{x}^{\text{in}} \approx \sum_{m=0}^K \theta_m T_m(\mathbf{L}) \mathbf{x}^{\text{in}}, \quad (28)$$

where $T_m(\mathbf{L}) \in \mathbb{R}^{N \times N}$ is the m order Chebyshev polynomial.

From another point of view, the convolution of the ChebyNet can be understood as the sum of polynomials of different orders evaluated at the Laplacian. If the order is m , the receptive field of the convolution is the m -ring neighborhood of a vertex. The ChebyNet is equivalent to the weighted sum of multiple convolutions with increasing receptive field. The problem of this convolution is that it is not resolution independent, because the size of the m -ring neighborhood depends on the discretization of the surface.

Our idea is to express \mathbf{w}_θ in a wavelet filter basis, rather than a polynomial basis. Please note that there is a difference between the wavelet filter basis and the wavelet basis. The wavelet filter basis is a basis in the spectral domain, but the wavelet basis exists in the spatial domain on the surface:

$$\mathbf{w}_\theta = \sum_{m=0}^K \theta_m \text{diag}(\{g_{t_m}(\lambda_j)\}_{j=0}^k) = \sum_{m=0}^K \theta_m g_{t_m}(\Lambda). \quad (29)$$

Now the convolution can be simplified as follows:

$$\mathbf{x}^{\text{out}} = \mathbf{y} * \mathbf{w} \mathbf{x}^{\text{in}} \approx \sum_{m=0}^K \theta_m \Psi_{t_m}^T \mathbf{x}^{\text{in}}, \quad (30)$$

where each matrix $\Psi_{t_m} \in \mathbb{R}^{N \times N}$ is composed of the wavelet basis with scale t_m .

In practice, there are three factors to consider. First, the magnitude of high frequency wavelet functions is very small, which leads to numerical robustness issues during learning the parameters. Second, we need to ensure that the convolution operation leads to similar results for surfaces that are discretized with different sampling densities. Therefore, to solve the first two issues, we perform L_1 normalization on the wavelet functions (i.e., normalize the columns of the wavelet matrix Ψ). Finally, we don't need to select all the filters, we only need to select a part (such as sampling about half) of the filters to reduce the calculation. Therefore, the new convolution is as follows,

$$\mathbf{x}^{\text{out}} = \mathbf{y} * \mathbf{w} \mathbf{x}^{\text{in}} \approx \sum_{t_s \in \mathcal{S}_{t_s}} \theta_{t_s} \overline{\Psi}_{t_s}^T \mathbf{x}^{\text{in}}, \quad (31)$$

where $\overline{\Psi}_{t_s}$ is a normalized matrix with each wavelet L_1 normalized, where the sum of the normalized wavelet is 1.

For the high-dimensional case with $\mathbf{X}^{\text{in}} \in \mathbb{R}^{N \times C}$, we form our convolution module by the following formula:

$$\mathbf{Z} = \text{Norm} \left(\text{ELU} \left(\sum_{t_s \in \mathcal{S}_{t_s}} \overline{\Psi}_{t_s}^T \mathbf{X}^{\text{in}} \mathbf{W}_{t_s} \right) \right). \quad (32)$$

where $\mathbf{W}_{t_s} \in \mathbb{R}^{C \times O}$ and O are the dimensions of the output feature, and $\text{Norm}()$ is a $\min - \max$ normalization on every dimensional feature to normalize energies of vertices. This module can be called as ‘‘MGCONV’’.

5.2 Network Architecture Details

The MGCONV layer described previously can be used to construct our MGCN. Here, we describe the architecture we used for descriptor learning. To learn a shape descriptor, we build an MGCN network by stacking 6 layers of MGCONV and one fully connected layer: $5 \times$



Fig. 7. Visualization of filters learned by our network. For one input mesh and one selected vertex on the head, we show 24 manually selected and normalized filters to ensure some variability. Note that the network learns about 60K filters so this is only a small subset. Further, the filters are normalized, since the range of values between different filters differs significantly.

MGCONV96(16) + MGCONV128(16) + FC256. MGCONV $x(k)$ refers to a convolutional layer that has an x -dimensional output of feature maps, and (k) refers to scale k of our wavelet scale set. and FC x refers to a fully connected layer that outputs a vector with x -dimension, and 256 refers to the 256 dimension of the output feature.

We also use a new loss to train the descriptor learning network, called HardNet loss [Mishchuk et al. 2017]. HardNet loss is used in the local descriptor generation of the image, and its advantage is that it can directly calculate the loss of N pairs by computing N triplet distances. We apply this loss to the task of learning shape descriptors. In order to speed up the training process, a classification network is first used to train the MGCN. One fully connected layer FCd is added after the last MGCONV layer, and cross-entropy loss is used to classify each point. Then, HardNet loss is used to directly train on MGCN to reduce the distance between positive examples and increase the distance between negative examples.

To give some intuition of the learned filters, we visualize a small subset of them in Fig. 7 for a training run on the FAUST dataset.

5.3 Discussion

Spectral CNN exploits the fact that the convolution in the time domain is equal to the product in the frequency domain, but this network leads to descriptors that are too smooth and do not contain enough local information. ChebyGCN uses k -order Chebyshev polynomials to expand filters in the frequency domain (Note that in this section k does not refer to the size of the Laplacian basis). GCN further simplifies ChebyGCN and uses a 1-ring neighborhood to approximate filters to reduce the amount of calculations. By contrast, SplineCNN and DGCNN belong to the class of networks using spatial convolution. The core questions of the spatial convolution method are how to find neighbors and how to aggregate the information from the neighbors. Comparing convolution in the frequency domain to the convolution in the spatial domain, it can be seen that

the locality is important to improve performance. But this locality also brings some problems. For example, GCN and SplineCNN use 1-ring neighborhood information. ChebyGCN uses k -order Laplacian polynomials, so it uses k -ring neighborhood information. DGCNN uses K -nearest neighbors in feature space to define the support of a convolution filter. However, such convolution operations do not generalize well to meshes of different resolution, because the size of a K - or 1-ring neighborhood (the receptive field of the filters) changes with the resolution of a mesh. An alternative method is to calculate a geodesic disk centered at each vertex and locally re-sample the surface [Wang et al. 2019a]. However, computing dense geodesic disk is time-consuming and resampling the surface introduces additional errors.

An alternative approach is the graph wavelet neural network of [Xu et al. 2019]. The formula for convolution is $\mathbf{y} *_g \mathbf{x} = \Psi \mathbf{g}_\theta \Psi^{-1} \mathbf{x}^{in}$. However, because the filter \mathbf{g}_θ has parameters equal to the number of vertices, the network only works for meshes with the same number of vertices. Second, the calculation of matrix inversion is very slow for large graphs. In summary, there is currently no reliable network to handle multi-resolution datasets.

In our MGCONV layer, we use many advantages of the nature of wavelets, but make important changes to the existing graph wavelet neural network. First, the spectral filters can be expressed in the wavelet filter basis. In the spatial domain, convolution operations are replaced by multiplying with a matrix composed of the wavelet basis. Because the wavelet basis functions are robust to the change of resolution and triangulation, our convolution also has the ability to cope with different resolutions. Second, due to the multiscale nature of the wavelet basis, we have the ability to simultaneously capture local and global information. Most importantly, we can capture local information without the explicit computation of local neighborhoods using geodesic distances as used in [Wang et al. 2019a].

6 EXPERIMENTAL RESULTS

We present multiple qualitative results. After describing the used evaluation metrics, we compare WEDS with other unsupervised descriptors, compare MGCN with other network architectures for descriptor learning, and evaluate different parameter settings. In our experiments, the results are obtained using an Intel Core i7-7700 processor with 4.2 GHz and 16 GB RAM. Offline training is run on an NVIDIA GeForce GTX RTX (24 GB memory) GPU.

6.1 Evaluation metrics

We use three metrics to evaluate descriptors: average geodesic error, cumulative geodesic error, and cumulative match characteristic. We report results for two types of ground truth matches: the closest vertex on the direct map and the closest vertex on the symmetric map.

–**Average geodesic error** is a scalar to compute the average per-vertex error. The direct error evaluates the geodesic error between a predicted vertex and its ground-truth correspondence. The symmetry-aware error is the minimum of the direct error and the error between predicted vertex and the symmetric ground truth. The predicted

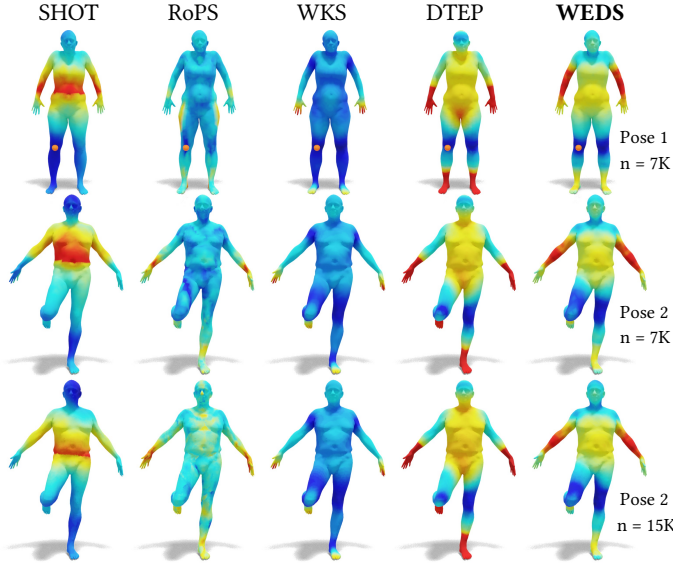


Fig. 8. For a selected vertex on the knee (shown in orange) we visualize the distance of the descriptor on the selected vertex to the descriptors of other vertices. A blue color indicates a small distance and a red color a large distance. Top row: descriptor distances on the same mesh. Second row: descriptor distances on a different mesh in the same resolution. Third row: descriptor distances on a different mesh in a different resolution. Form left to right: SHOT, RoPS, WKS, DTEP, and WEDS. We can observe that WEDS and DTEP are more discriminative than WKS and that SHOT and RoPS are not resolution independent.

vertex is obtained by computing the nearest-neighbor using the L2 distance in feature space.

–**Cumulative geodesic error (CGE)** measures matching quality by plotting the percentage of nearest-neighbor correspondences that are at most r -geodesically distant from the ground-truth correspondence. According to the type of ground truth used, CGE is also divided into direct CGE and symmetry-aware CGE.

–**Cumulative match characteristic (CMC)** evaluates the percentage of vertices that find a correct match among the k -nearest neighbors in the descriptor space. According to the type of ground truth used, CMC is also divided into direct CMC and symmetry-aware CMC.

For the network evaluation, we use the descriptor evaluation if the network is used for learning descriptors.

6.2 Unsupervised Descriptor Evaluation

We first analyze the discriminative power of descriptors. To verify the effectiveness of the proposed local descriptor, we choose FAUST [Bogo et al. 2014] and SCAPE [Angelov et al. 2005] as our test datasets. We also use an extended version of FAUST [Wang et al. 2019a], which contains meshes with different resolution, triangulation, scale, and rotation. As competitors, we select three spatial domain descriptors (SI [Johnson and Hebert 1999], SHOT [Tombari et al. 2010], RoPS [Guo et al. 2013]) and four spectral domain descriptors (HKS [Sun et al. 2010], WKS [Aubry et al. 2011], LPS [Wang et al. 2019a], and DTEP [Melzi et al. 2018]).

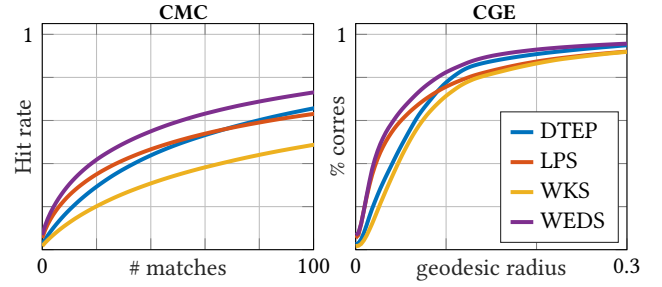


Fig. 9. The symmetric CMC and CGE metrics of unsupervised descriptors on the FAUST dataset. We use different line colors to indicate different networks. Note that our WEDS descriptor is the most discriminative especially according to the CMC curves.

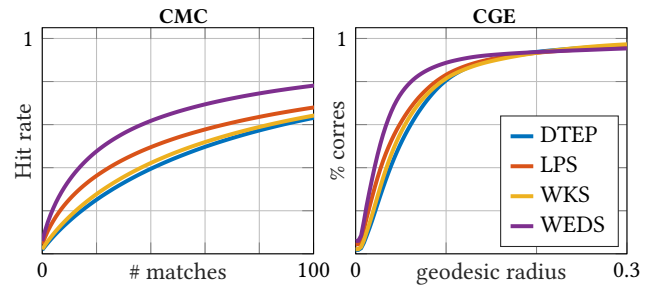


Fig. 10. The symmetric CMC and CGE metrics of unsupervised descriptors on the SCAPE dataset. We use different line colors to indicate different networks. Note that our WEDS descriptor is the most discriminative especially according to the CMC curves.

We conduct an extensive evaluation for different unsupervised descriptors on FAUST and SCAPE. Between different human, the pairs are isometric or non-isometric. To reduce variability for fair test, we selected 15 models on two datasets randomly and test every two pairs of fifteen models. The total number of tested pairs is 15×14 . Table 2 shows the average geodesic error A/B on 15×14 pairs. A is direct error and B is symmetry-aware error.

From Table 2, we find that RoPS is the better among the spatial domain descriptors, but the geodesic error is still large. The results show that spatial domain descriptors can not handle non-rigid matching well. In addition to HKS being too smooth, frequency domain descriptors have better performance. Among the frequency domain descriptors, WEDS has best discrimination among state-of-the-art descriptors two datasets and has about 10% performance improvement. A visualization of the distance of the descriptor of a selected vertex to other vertices' descriptors is shown in Fig. 8. More details in the form of curves are provided in Fig. 9 and Fig. 10. Here we see that the improvement of the CMC metric is even more significant than the average geodesic error. Other tests are in additional materials.

6.3 Graph Network Evaluation

To test the effectiveness of the network, we first test the shape descriptors that have been further improved by the network. The network structure is described in Section 5.2.

Table 2. Average geodesic error ($\times 10^{-3}$) computed on 15×14 shape pairs with different descriptors. We report the error in the form (direct error / symmetry-aware error). WEDS improves about 10% compared to the best competitor.

Descriptors	Dataset	
	FAUST(6890)	SCAPE(12.5K)
SI	352 / 153	380 / 251
SHOT	490 / 412	447 / 369
RoPS	346 / 252	267 / 187
HKS	511 / 396	507 / 409
WKS	335 / 118	260 / 72
LPS	325 / 97	227 / 71
DTEP	312 / 89	267 / 76
WEDS	287 / 69	225 / 66

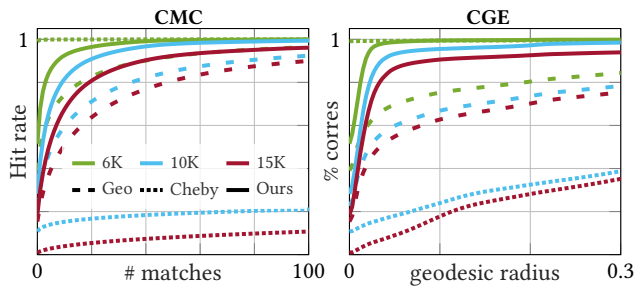


Fig. 11. The direct CMC and CGE metrics of learned descriptors on the FAUST dataset. We use different *line types* to indicate different networks, where the Geo-based network [Wang et al. 2019a] is in dashed lines, the ChebyCNN is in dotted lines, and our MGCN is in solid lines. We use different *colors* to indicate different resolutions on the target shapes. Note that other networks do not generalize to different resolution as well as our network.

6.3.1 Descriptor learning task. In this task, we focus on learning robust descriptors on different resolution. In addition to the data previously introduced, to test the influence of different resolution, we also introduce SCAPE 5K dataset. The vertex position and triangulation are totally different. We have a ground-truth correspondence between the remeshed vertex and 5000 points sampled from the original dataset. There are not many shape descriptor learning approaches considering different resolutions. One of papers used Geodesic-based networks embedded LPS [Wang et al. 2019a] to achieve the effect of training at one resolution and testing at another resolution with too much decline. Three unsupervised descriptors (WKS, LPS, WEDS) are selected. We set feature dimension 128 for fair comparison on network. For network comparison, we choose the most competitive methods (CGF32 [Khoury et al. 2017], OSD [Litman and Bronstein 2014], SplineCNN(1-neighborhood) [Fey et al. 2018] and Geodesic-based networks [Wang et al. 2018]). We also build a network stacked by ChebyGCN(k-neighborhood) [Defferrard et al. 2016] layers. The structure is followed by Section 5.2, we replace MGCONV layers with ChebyGCN layers. The rest of the structure such as input and output dimension is the same as MGCN. **Experimental results on FAUST.** In this setting, all the combinations for learning descriptors are generated by learning only on FAUST 6890 vertices and testing on FAUST 6890 and other vertices. We use the nearest neighbor of the feature space to detect

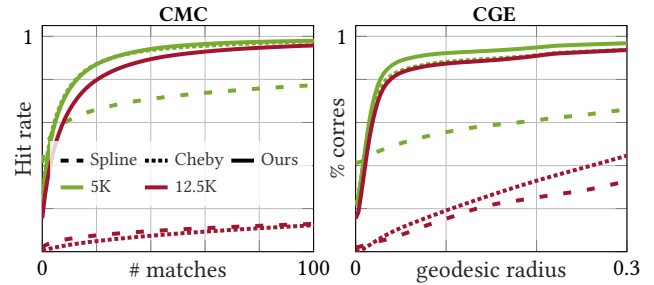


Fig. 12. The direct CMC and CGE metrics of learned descriptors on the SCAPE dataset. We use different *line types* to indicate different networks and different *colors* to indicate different resolutions on the target shapes. Note that other networks do not generalize to different resolution as well as our network.

Table 3. Average geodesic error ($\times 10^{-3}$) computed on 15×14 shape pairs of FAUST with different descriptors. We report the error in the form (direct error / symmetry-aware error). WEDS + MGCN significantly improves upon the best previous work LPS + Geo-based.

Descriptors	Network	#Resolution		
		6890 - 6890	6890 - 10K	6890 - 15K
Histogram	CGF	424 / 298	433 / 300	460 / 332
-	OSD	398 / 182	457 / 254	430 / 221
-	SplineCNN	276 / 161	488 / 378	524 / 438
WEDS	ChebyGCN	6 / 1	527 / 387	551 / 377
WKS	Geo-based	204 / 35	221 / 52	252 / 69
LPS	Geo-based	164 / 22	203 / 43	223 / 55
WEDS	Geo-based	147 / 24	207 / 34	239 / 39
WKS	MGCN	19 / 13	88 / 34	124 / 69
LPS	MGCN	18 / 12	44 / 24	84 / 39
WEDS	MGCN	8 / 7	26 / 18	66 / 34

the matching discrimination of descriptors between different resolutions. Table 3 shows the average geodesic errors on different settings. It can be seen that the ChebyGCN network significantly overfits and the performance drops by a factor of about 100 if the resolution changes. SplineCNN was designed to directly learn a mapping between points of different shapes, so that we had to make modifications to use SplineCNN for descriptor learning: we take the output of the second to last linear mapping layer as the descriptor to learn. In general, we can observe that the performance of SplineCNN, CGF, and OSD is significantly worse than our MGCN. Based on the results we consider the geodesic-based network to be our main competitor. Similar to our network, the geodesic-based network is fairly robust to different surface discretizations, however, overall our results are much stronger. For example, the direct error is 3 to 18 times lower when our network is used across different resolutions. Fig. 11 reports the curves for the CMC and CGE metric of different descriptors. Therefore, MGCN utilizes GCN’s powerful fitting capabilities and guarantees robustness at different resolutions simultaneously. In addition, using different descriptors as input will also affect the network. The results shows that the performance of the setting of WEDS and MGCN is the best.

Experimental results on SCAPE. The same network may behave differently on different datasets, we need another dataset to test

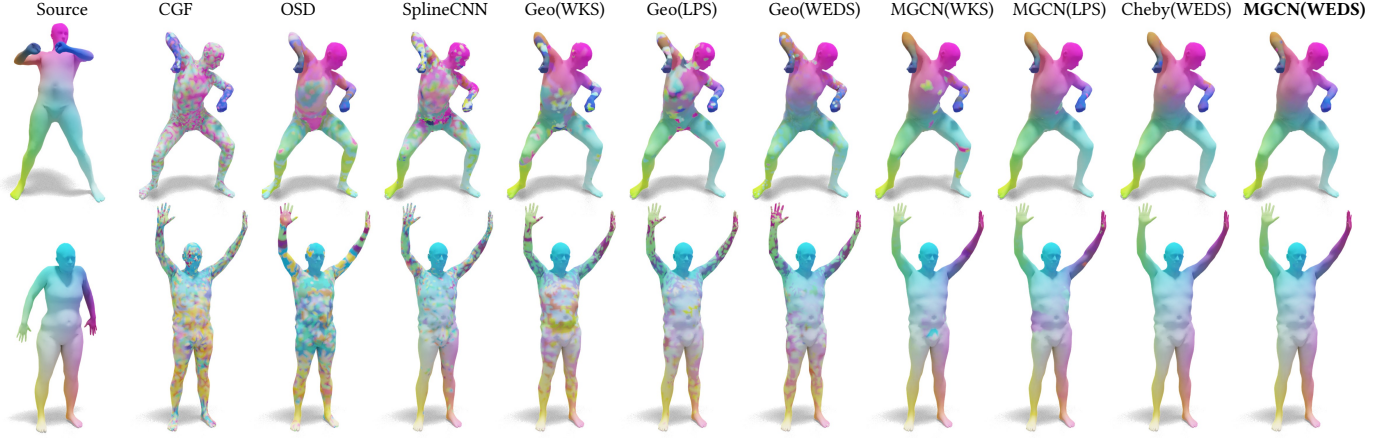


Fig. 13. Here we shown an example pair from SCAPE (top row) and FAUST (bottom row), where the source and the target shape has the same resolution and we compare the maps obtained from different methods visualized by color transfer. The descriptor input of a network is shown inside brackets.

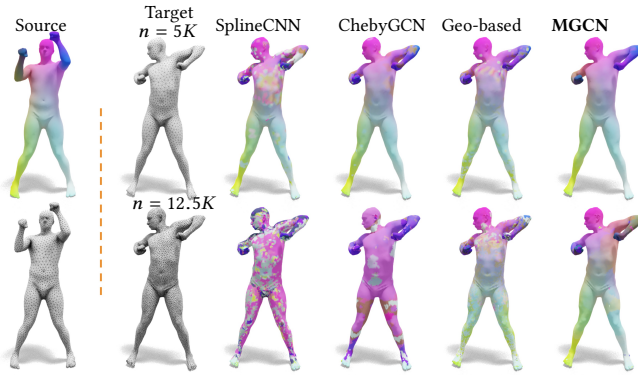


Fig. 14. Here we compare the performance of different methods w.r.t. different resolutions. The source shape has 5K vertices and the target shape has 5K vertices in the top row and 12K vertices in the bottom row. All the networks take WEDS as input. Note that the matches change considerably from the top row to the bottom row for all networks except our proposed MGCN. This indicates that our network can greatly improve upon the generalization performance of the current state of the art.

the network. In this setting, all the combinations for learning descriptors are generated by learning only on SCAPE 5K vertices and testing on SCAPE 5K and 12.5K vertices. We then perform feature matching between different resolutions. SCAPE 5K and 12.5K have a completely different shape structure, which is more difficult. Table 4 shows average geodesic errors on different settings. Compared with FAUST dataset, OSD has better results on SCAPE, but it seems that overfitting is more severe at resolutions. The descriptors of CGF still perform poorly on the mesh. Same as FAUST, SplineCNN and ChebyGCN overfit at one resolution. Geodesic-based method seems to be more stable with the change of resolution on FAUST, but the discrimination of descriptor is difficult to improve further. The setting of WEDS and MGCN still generates the most discriminative descriptor, while ensuring robustness to the change of resolution. Fig. 12 shows the curves for the CMC and CGE metric of different descriptors. Compared with SplineCNN and ChebyGCN, MGCN outputs better performing descriptors that are more robustness at different resolutions. This is also illustrated by Fig. 6, where we visualize the learned descriptors of SplineCNN and MGCN.

Table 4. Average geodesic error ($\times 10^{-3}$) computed on 10×9 shape pairs of SCAPE with different descriptors. We report the error in the form (direct error / symmetry-aware error). MGCN outperforms its best competitors ChebyGCN and Geo-based by a large margin.

Descriptors	Network	#Resolution	
		SCAPE 5K	SCAPE 5K-12.5K(Test)
Histogram	CGF	374 / 264	428 / 323
-	OSD	259 / 94	835 / 742
-	SplineCNN	297 / 180	503 / 353
WEDS	ChebyGCN	68 / 29	458 / 332
WKS	Geo-based	185 / 72	192 / 80
LPS	Geo-based	175 / 68	182 / 74
WEDS	Geo-based	163 / 65	179 / 71
WKS	MGCN	67 / 46	98 / 64
LPS	MGCN	54 / 26	82 / 44
WEDS	MGCN	48 / 17	73 / 39

Fig. 13 shows a qualitative example of a pair of FAUST shapes and SCAPE shapes, where we use the learned descriptors to find correspondences and compare the quality of the obtained maps between different competitors. Another comparison of the performance of different methods w.r.t. different resolutions is given in Fig. 14. In both figures, we can observe that our learned descriptor generated by MGCN leads to the best maps.

6.4 Parameter Settings

Different parameters will affect the performance of different descriptors. In order to compare fairly, we need to choose the best parameters for each descriptor. We focus on the spectral descriptors such as HKS, WKS, DTEP. For other descriptors, because of the variety of parameters, we use the parameters recommended by the authors. The usual parameters of these spectral descriptors mainly include three, which are the number of eigenfunctions, the number of feature scale and the number of dimension we sample. We test on 6 models with 6×5 pairs to select all the parameters. First, we choose the number of eigenfunctions, and then we fix function and select the number of scale. Finally, we uniformly sample on the scale to obtain the best descriptors.

The number of eigenfunctions. We pick two feature scales 96 and 128 to choose the number of eigenfunctions. Each descriptor is

Table 5. Average geodesic error ($\times 10^{-3}$) computed on 6×5 shape pairs of FAUST with different descriptors. We report the error in the form (direct error / symmetry-aware error).

Descriptors (#96)	#Basis			
	50	100	200	300
HKS	500 / 382	500 / 381	501 / 382	501 / 382
WKS	341 / 152	325 / 112	358 / 139	339 / 118
DTEP	374 / 208	302 / 95	295 / 100	366 / 146
WEDS	352 / 110	236 / 83	263 / 68	256 / 77

Table 6. Average geodesic error ($\times 10^{-3}$) computed on 6×5 shape pairs of FAUST with different descriptors. We report the error in the form (direct error / symmetry-aware error).

Descriptors (#128)	#Basis			
	50	100	200	300
HKS	503 / 383	502 / 383	501 / 382	502 / 384
WKS	334 / 134	322 / 112	336 / 126	355 / 115
DTEP	397 / 226	307 / 96	310 / 100	377 / 158
WEDS	364 / 126	262 / 85	257 / 65	248 / 69

computed with the input of the two feature scales and four kind of number of eigenfunctions, which is 50, 100, 200, and 300. Table 5 and Table 6 shows the average geodesic error when selecting four kinds of eigenfunctions with 96 and 128 feature scales. HKS and WKS have 4 best results with 100 eigenfunctions. DTEP has 3 best results with 100 eigenfunctions and 1 best results with 200 eigenfunctions. WEDS has 2 best results with 300 eigenfunctions. 1 best results with 100 and 200 eigenfunctions each. Therefore, We pick HKS:100, WKS:100, DEP: 100, WEDS: 300 as the number of eigenfunctions. From this aspect, it can be seen that our descriptors seem to have better performance with more eigenfunctions, while other frequency-domain descriptors do not perform better with more eigenfunctions. One possible explanation is that when constructing the descriptor, the vertex information needs to be reconstructed by the basis function, so more basis functions may lead to higher reconstruction accuracy, so that the descriptor representing the shape can be better generated.

The number of feature scale. We fix the number of eigenfunctions and choose the number of feature scale. We choose the number of scales from small to large until the best result is selected. Scale in WEDS means Num, which is the feature dimension of output. Table 7 shows the average geodesic error under different scale.

In the same way as selecting the eigenfunctions, we choose HKS:64, WKS:96, DEP: 96, WEDS: 1024 as the number of scale. Our descriptor is different from other descriptors, the difference is that the higher the dimension of our descriptor is, the better the performance is. It is because Num of WEDS is related to the number of wavelet scales. As with the number of eigenfunctions, the larger the number of scales is, the better the accuracy of the signal reconstruction is, so leads to better performance of our descriptor.

The number of sample. We fix the number of eigenfunctions and the number of feature scale. The features are sampled uniformly, and we show the average geodesic error in the Table 8, we pick HKS:16(64), WKS:16(96), DEP: 96(96), WEDS: 1024(1024) as the number of sample, the first number and second are feature dimension

after and before sampling. From this table, WEDS has a great improvement when the sampling number is 128. Therefore, we choose 128 as the feature dimension that we input into the network.

The time of descriptors. We also compared the computation time of the four spectral descriptors. The increase in performance is often accompanied by a decrease in computing efficiency. We choose the recommended parameters of these four spectral methods. And the computation cost is shown in Table 9. It can be seen that LPS and DTEP have improved performance compared to traditional spectral descriptors, but it takes a lot of time because of the computation of geodesic disks and optimization. WEDS can reduce time consumption while achieving the best performance by energy decomposition.

6.5 Limitations and Future Work

There are still important challenges left for future work. First, we suspect that our descriptor learning solution still overfits the training data too much, since there is not enough variability in current shape matching datasets. The most beneficial and practical future work would therefore be to collect larger training datasets with more variability. Second, our current implementation and evaluation is limited so meshes. It would be interesting to extend our work to point clouds and triangle soups in future work.

7 CONCLUSIONS

We proposed a novel framework for computing two types of shape descriptors: 1) the unsupervised descriptor WEDS is computed by using graph wavelets to decompose the Dirichlet energy on a surface. 2) WEDS can be refined by our proposed MGCN to yield a learned descriptor. Our results show that the new descriptor WEDS is more discriminative than the current state-of-the-art non-learned descriptors and that the combination of WEDS and MGCN is better than the state-of-the-art learned descriptors. An important attribute of descriptors is the robustness to different surface discretizations. Our results demonstrate that MGCN generalizes significantly better to different surface discretizations than previous work.

In this paper, we proposed a descriptor learning framework including a new descriptor and a graph neural network. We first verified that *wavelet energy decomposition signature* (WEDS) is robust to resolution, rigid transformations, and is also a discriminative descriptor. Then *multiscale graph convolutional network* (MGCN) was proposed to improve the discrimination of unsupervised descriptors. Most importantly, MGCN can maintain robustness to the change of resolution while improving discrimination. Our framework was demonstrated by comparing to several recent state-of-the-art descriptors and neural networks. Our framework not only improved the performance of the descriptor, but also maintained the robustness to resolution while improving the discrimination of the descriptor. In addition to descriptor learning, our network was used for semi-supervised node classification and achieved competitive classification accuracy.

REFERENCES

- Dragomir Anguelov, Praveen Srinivasan, Daphne Koller, Sebastian Thrun, Jim Rodgers, and James Davis. 2005. SCAPE: shape completion and animation of people. *ACM Trans. on Graphics (Proc. SIGGRAPH)* 24, 3 (2005), 408–416.

Table 7. Average geodesic error ($\times 10^{-3}$) computed on 6x5 shape pairs of FAUST with different descriptors. We report the error in the form (direct error / symmetry-aware error).

Descriptors	#Scale									
	16	32	64	96	128	192	256	512	768	1024
HKS	508 / 390	499 / 379	495 / 37	500 / 381	502 / 383	506 / 387	510 / 390	-	-	-
WKS	469 / 290	539 / 371	350 / 142	325 / 112	332 / 112	335 / 117	337 / 120	-	-	-
DTEP	305 / 105	311 / 93	305 / 91	302 / 95	307 / 96	304 / 89	305 / 89	-	-	-
WEDS*	290 / 100	269 / 85	257 / 78	256 / 77	248 / 69	247 / 68	245 / 65	244 / 62	245 / 62	244 / 59

Table 8. Average geodesic error ($\times 10^{-3}$) computed on 6x5 shape pairs of FAUST with different descriptors. We report the error in the form (direct error / symmetry-aware error).

Descriptors	#Feature			
	16	32	64	96
HKS	486 / 367	489 / 369	495 / 375	-
WKS	323 / 111	325 / 109	323 / 111	325 / 112
DTEP	309 / 98	305 / 96	304 / 95	302 / 95
WEDS	295 / 96	305 / 103	268 / 69	286 / 71
	128	256	512	1024
	250 / 66	253 / 59	250 / 62	244 / 59

Table 9. The computation time of different unsupervised descriptors.

Time(s)	#Resolution					
	5K	6890	8K	10K	12K	15K
HKS	0.21	0.23	0.27	0.31	0.36	0.41
WKS	0.27	0.31	0.33	0.36	0.41	0.47
LPS	185	464	655	1090	1482	2174
DTEP	1124	1467	1659	2025	2235	2639
WEDS	16.6	24.7	42.2	65.7	82.5	144.3

Mathieu Aubry, Ulrich Schlickewei, and Daniel Cremers. 2011. The wave kernel signature: A quantum mechanical approach to shape analysis. In *IEEE International Conference on Computer Vision Workshops (ICCV Workshops)*. IEEE, 1626–1633.

Federica Bogo, Javier Romero, Matthew Loper, and Michael J Black. 2014. FAUST: Dataset and evaluation for 3D mesh registration. In *IEEE Computer Vision and Pattern Recognition (CVPR)*. 3794–3801.

Davide Boscaini, Jonathan Masci, Simone Melzi, Michael M. Bronstein, Umberto Castellani, and Pierre Vandergheynst. 2015. Learning class-specific descriptors for deformable shapes using localized spectral convolutional networks. *Computer Graphics Forum* 34, 5 (2015), 13–23.

Davide Boscaini, Jonathan Masci, Emanuele Rodolà, Michael M Bronstein, and Daniel Cremers. 2016. Anisotropic diffusion descriptors. *Computer Graphics Forum* 35, 2 (2016), 431–441.

Michael M Bronstein, Joan Bruna, Yann LeCun, Arthur Szlam, and Pierre Vandergheynst. 2017. Geometric deep learning: going beyond euclidean data. *IEEE Signal Processing Magazine* 34, 4 (2017), 18–42.

Michael M Bronstein and Iasonas Kokkinos. 2010. Scale-invariant heat kernel signatures for non-rigid shape recognition. In *IEEE Computer Vision and Pattern Recognition (CVPR)*. IEEE, 1704–1711.

Joan Bruna, Wojciech Zaremba, Arthur Szlam, and Yann Lecun. 2014. Spectral networks and locally connected networks on graphs. In *International Conference on Learning Representations (ICLR2014)*, CBL5, April 2014.

Michaël Defferrard, Xavier Bresson, and Pierre Vandergheynst. 2016. Convolutional neural networks on graphs with fast localized spectral filtering. In *Advances in neural information processing systems*. 3844–3852.

Haowen Deng, Tolga Birdal, and Slobodan Ilic. 2018. Ppfnnet: Global context aware local features for robust 3d point matching. In *Proceedings of the IEEE Conference on Computer Vision and Pattern Recognition*. 195–205.

Matthias Fey, Jan Eric Lenssen, Frank Weichert, and Heinrich Müller. 2018. SplineCNN: Fast geometric deep learning with continuous B-spline kernels. In *Proceedings of the IEEE Conference on Computer Vision and Pattern Recognition*. 869–877.

Andrea Frome, Daniel Huber, Ravi Kolluri, Thomas Bülow, and Jitendra Malik. 2004. Recognizing objects in range data using regional point descriptors. In *European Conference on Computer Vision (ECCV)*. Springer, 224–237.

Yulan Guo, Ferdous Sohel, Mohammed Bannamoun, Min Lu, and Jianwei Wan. 2013. Rotational projection statistics for 3D local surface description and object recognition. *Int. Journal of Computer Vision* 105, 1 (2013), 63–86.

David K Hammond, Pierre Vandergheynst, and Rémi Gribonval. 2011. Wavelets on graphs via spectral graph theory. *Applied and Computational Harmonic Analysis* 30, 2 (2011), 129–150.

Haibin Huang, Evangelos Kalogerakis, Siddhartha Chaudhuri, Duygu Ceylan, Vladimir G Kim, and Ersin Yumer. 2018. Learning Local Shape Descriptors from Part Correspondences with Multiview Convolutional Networks. *ACM Trans. on Graphics* 37, 1 (2018), 6.

A. E. Johnson and M. Hebert. 1999. Using spin images for efficient object recognition in cluttered 3D scenes. *IEEE Trans. on Pattern Analysis and Machine Intelligence* 21, 5 (May 1999), 433–449. <https://doi.org/10.1109/34.765655>

Marc Khoury, Qian-Yi Zhou, and Vladlen Koltun. 2017. Learning compact geometric features. In *IEEE Computer Vision and Pattern Recognition (CVPR)*. 153–61.

Thomas N. Kipf and Max Welling. 2017. Semi-Supervised Classification with Graph Convolutional Networks. In *International Conference on Learning Representations (ICLR)*.

Roei Litman and Alexander M Bronstein. 2014. Learning spectral descriptors for deformable shape correspondence. *IEEE Trans. on Pattern Analysis and Machine Intelligence* 36, 1 (2014), 171–180.

Jonathan Masci, Davide Boscaini, Michael Bronstein, and Pierre Vandergheynst. 2015. Geodesic convolutional neural networks on riemannian manifolds. In *IEEE International Conference on Computer Vision Workshops (ICCV Workshops)*. 37–45.

Majid Masoumi and A Ben Hamza. 2017. Spectral shape classification: A deep learning approach. *Journal of Visual Communication and Image Representation* 43 (2017), 198–211.

Simone Melzi, Maks Ovsjanikov, Giorgio Roffo, Marco Cristani, and Umberto Castellani. 2018. Discrete time evolution process descriptor for shape analysis and matching. *ACM Trans. on Graphics* 37, 1 (2018), 4.

Anastasia Mishchuk, Dmytro Mishkin, Filip Radenovic, and Jiri Matas. 2017. Working hard to know your neighbor’s margins: Local descriptor learning loss. In *Advances in Neural Information Processing Systems*. 4826–4837.

Martin Reuter, Franz-Erich Wolter, and Niklas Peinecke. 2006. Laplace–Beltrami spectra as ‘Shape-DNA’ of surfaces and solids. *Computer-Aided Design* 38, 4 (2006), 342–366.

Raif M Rustamov. 2007. Laplace–Beltrami eigenfunctions for deformation invariant shape representation. In *Proc. of Symp. of Geometry Processing*. Eurographics Association, 225–233.

Ljubiša Stanković and Ervin Sejdić. 2019. *Vertex-frequency analysis of graph signals*. Springer.

Jian Sun, Maks Ovsjanikov, and Leonidas J. Guibas. 2010. A Concise and Provably Informative Multi-Scale Signature Based on Heat Diffusion. *Computer Graphics Forum* 28, 5 (2010), 1383–1392.

Federico Tombari, Samuele Salti, and Luigi Di Stefano. 2010. Unique signatures of histograms for local surface description. In *European Conference on Computer Vision (ECCV)*. Springer, 356–369.

Hanyu Wang, Jianwei Guo, Dong-Ming Yan, Weize Quan, and Xiaopeng Zhang. 2018. Learning 3D Keypoint Descriptors for Non-rigid Shape Matching. In *European Conference on Computer Vision (ECCV)*. Springer, 3–20.

Yiqun Wang, Jianwei Guo, Dong-Ming Yan, Kai Wang, and Xiaopeng Zhang. 2019a. A Robust Local Spectral Descriptor for Matching Non-Rigid Shapes With Incompatible Shape Structures. In *The IEEE Conference on Computer Vision and Pattern Recognition (CVPR)*. 6231–6240.

Yue Wang, Yongbin Sun, Ziwei Liu, Sanjay E Sarma, Michael M Bronstein, and Justin M Solomon. 2019b. Dynamic graph cnn for learning on point clouds. *ACM Transactions on Graphics (TOG)* 38, 5 (2019), 1–12.

Lingyu Wei, Qixing Huang, Duygu Ceylan, Etienne Vouga, and Hao Li. 2016. Dense human body correspondences using convolutional networks. In *IEEE Computer Vision and Pattern Recognition (CVPR)*. 1544–1553.

Bingbing Xu, Huawei Shen, Qi Cao, Yunqi Qiu, and Xueqi Cheng. 2019. Graph Wavelet Neural Network. In *ICLR (Poster)*. OpenReview.net.

Andrei Zaharescu, Edmond Boyer, Kiran Varanasi, and Radu Horaud. 2009. Surface feature detection and description with applications to mesh matching. In *IEEE Computer Vision and Pattern Recognition (CVPR)*. IEEE, 373–380.

Andy Zeng, Shuran Song, Matthias Nießner, Matthew Fisher, Jianxiong Xiao, and Thomas Funkhouser. 2017. 3dmatch: Learning local geometric descriptors from rgb-d reconstructions. In *IEEE Computer Vision and Pattern Recognition (CVPR)*. IEEE,

199–208.

A ADDITIONAL RESULTS

In this appendix, we give a proof for the reconstruction capabilities of our wavelet filter basis.

$$\sum_{m=0}^K \sum_{\nu} a(\nu)^{-1} W_{\mathbf{f}}(t_m, \nu) \psi_{t_m, \nu} \quad (33)$$

$$= \sum_{m=0}^K \sum_{\nu} a(\nu)^{-1} \sum_{j=0}^{N-1} a(\nu) g_{t_m}(\lambda_j) \sigma_j \phi_j(\nu) \sum_{j=0}^{N-1} a(\nu) g_{t_m}(\lambda_j) \phi_j(\nu) \phi_j \quad (34)$$

$$= \sum_{m=0}^K \sum_{i=0}^{N-1} g_{t_m}(\lambda_i) \sigma_i \sum_{j=0}^{N-1} g_{t_m}(\lambda_j) \phi_j \sum_{\nu} \phi_i(\nu) a(\nu) \phi_j(\nu) \quad (35)$$

$$= \sum_{m=0}^K \sum_{j=0}^{N-1} g_{t_m}^2(\lambda_j) \sigma_j \phi_j \quad (i = j) \quad (36)$$

$$= \sum_{j=0}^{N-1} \sigma_j \phi_j \quad (\text{If } \sum_{m=0}^K g_{t_m}^2(\lambda_j) = 1 \text{ Parseval frame}) \quad (37)$$

$$= \mathbf{f} \quad (38)$$